DOI: 10.31401/WS.2025.proc.05

3D Speed Reconstruction of CME Events during Solar Cycle 24

Hedz S.[1], Tsvetkov Ts.[2]

[1]Independent Researcher
[2]Institute of Astronomy and National Astronomical Observatory, Bulgarian Academy of Sciences, Sofia, Bulgaria
tstsvetkov@astro.bas.bg

Abstract

Coronal mass ejections (CMEs) are a form of solar activity that has a major influence on space weather and requires further investigation of its properties. Calculating their 3D velocities allows for better understanding of their origin and true structure. We analyzed the correlation between the 2D velocities measured by SOHO/LASCO observations and the 3D velocities of 14 events of solar cycle 24, reconstructed using the StereoCAT online tool that allows simultaneous multi-instrumental measurements. Despite our relatively small sample and that StereoCAT analysis is subject to limitations, including human selection of tie-points, varying spacecraft viewing geometries, and incomplete data coverage for some events, we found extremely strong relationship between projected and "true" velocity of explored CMEs.

Keywords: coronal mass ejections; corona; magnetic fields

1. Introduction

CMEs constitute sudden expulsions of dense clouds of plasma from the outer atmosphere of the Sun. The various origins of CMEs include solar flares (SFs), eruptive prominences and nonequilibrium magnetic field configurations [Wagner, 1984]. CMEs as a phenomenon were first observed in 1971, which makes them a relatively recent discovery. The projected onto the plane of sky speeds of CMEs can range from less than 100 km s^{-1} to 2000 km s^{-1} [Yurchyshyn et al., 2005]. Occasionally their speeds may reach values up to 3 500 km s-1 [Chen, 2011]. The mean CME speed varies between 300 km s^{-1} (near solar minimum) and 500 km s^{-1} (near maximum of the solar cycle) [Yashiro et al., 2004]. Early CME speed measurements revealed two general profiles: slow CMEs, usually linked to eruptive prominences, and fast CMEs, associated with ARs [Gosling et al., 1976]. Sheeley et al. (1999) later classified CMEs into two types: gradual CMEs (400–600 km s^{-1}), associated with prominences, and impulsive CMEs (≥750 km s^{-1}), associated with SFs. However, CME speed-height profiles form a continuous distribution rather than two distinct groups [Low and Zhang, 2002].

CMEs occur at a varying rate throughout the solar cycle. NASA's Coordinated Data Analysis Workshop (CDAW) CMEs frequency rate during solar cycle (SC) 23 was ∼ 0.5 CMEs/day at solar minimum and ∼ 6 CMEs/day near solar maximum [Chen, 2011]. During the solar cycles 23 and 24 the mean speed of CMEs as observed by LASCO was found to be 360 km s^{-1}.

Active regions (ARs) are generally known to power solar eruptions due to the quantity of magnetic energy stored in them and free energy accumulated in the photosphere [Kontogiannis, 2022]. Additionally, ARs are a crucial part of identifying the evolution of the solar magnetic field as the cause for all types of solar activity. ARs vary in sizes and occur as a result of local magnetic anomalies due to the processes related to the solar dynamo mechanism [Weber et al., 2023]. The size of ARs, along with complexity and strength do not correlate with the kinematic properties of CMEs. They do, however increase the ARs' capability to produce active events, including CMEs. It has been proved for 84% of the 32 CME events investigated in a study by Subramanian and Dere (2001) to have an AR as their source. Another study carried out by

Wang and Zhang (2008) came to the conclusion that only 3% of ARs tend to produce fast CME events, regardless of using an alternative AR catalog based on SOHO/MDI synoptic charts.

The aim of this study is to evaluate the 3D parameters of CMEs and estimate if they can give us a better insight of their properties and propagation than the most commonly used 2D velocities. 3D reconstruction of CMEs is done using a variety of techniques, such as forward modeling, tie-pointing and triangulation, constraint on the mass calculation, polarization ratio, etc. [Mierla et al., 2010]. The 3D velocities of CMEs can be calculated by combining measurements provided by multiple spacecrafts. The correlation between the values of 3D and 2D speeds of CMEs is found to be high with the mean coefficient of determination being ∼68% [Tsvetkov et al., 2019].

CMEs are known to alter space weather as their sub-structures can in many cases cause geomagnetic storms [Gopalswamy, 2016]. Upon CME events happening, the ejected substance from the solar corona interacts with planets including Earth. CMEs may impact the environment and human activity regarding technology and sometimes be dangerous to our planet. This makes the study of CMEs essential as it is needed to be able to predict space weather alternations most precisely in the future.

2. Instruments

For this study, observations done by the Solar Terrestrial Relation Observatory (STEREO) and the Solar and Heliospheric Observatory (SOHO) are used as the primary source of data for CME analysis.

STEREO mission includes two identical space-borne observatories, situated at different points of Earth’s orbit ahead (STEREO A) and behind (STEREO B) our planet. COR1 and COR2 instruments are visible light Lyot coronagraphs and are part of the SECCHI instrument suite. The opportunities for CME research created by STEREO include accessing stereographic imagery of CMEs, exploring the magnetic origins of CMEs, investigating of their physical evolution, and observing geo-effective CMEs. In the study the data from STEREO COR2 is used, the field of view of the instrument being 15 solar radii with an inner limit of 2.5 solar radii [Howard et al., 2008].

The SOHO mission’s primary objective is the investigation of the Sun’s interior, as well as the solar wind and its acceleration. The SOHO spacecraft is equipped with helioseismology, coronal, and solar wind measurement instruments. The LASCO (Large Angle and Spectrometric Coronagraph) consists of three coronagraphs: C1, C2, and C3. For the purposes of the study, we are using the data from the C2 and C3 instruments. C2’s field of view is 1.5 to 6 solar radii, and C3’s is 3 to 30 solar radii [Domingo et al., 1995].

For combining and analyzing the data, as well as calculating CME kinematic properties, the Stereo CME Analysis Tool (StereoCAT) web app is utilized. For the initial selection of events as well as the comparison between the “projected” and the “true” velocities data from the SOHO/LASCO CME Catalog[1] are used.

3. Results

For this study, a total of 14 CME events was analyzed and their 3D velocities estimated using the StereoCAT tool. All of the utilized events took place during the Solar Cycle 24 (2008-2019), 50% (7/14 CMEs) of them being related to ARs, of which 4 CMEs can be associated with more than one AR. On the other hand, only 2/14 CMES (14%) are associated with SFs.

[1] https://cdaw.gsfc.nasa.gov/CME_list/

Our sample includes relatively low number of events with speeds mostly lying in the range between 200-600 km s^{-1}. The distribution of the 2D velocities, as measured by SOHO/LASCO CME Catalog is shown on Figure 1. According to Sheeley et al. (1999), most of the events included in our study (12/14) are gradual CMEs and only 2/14 are impulsive, despite one of the latter (2013/11/02) not being associated with SF.

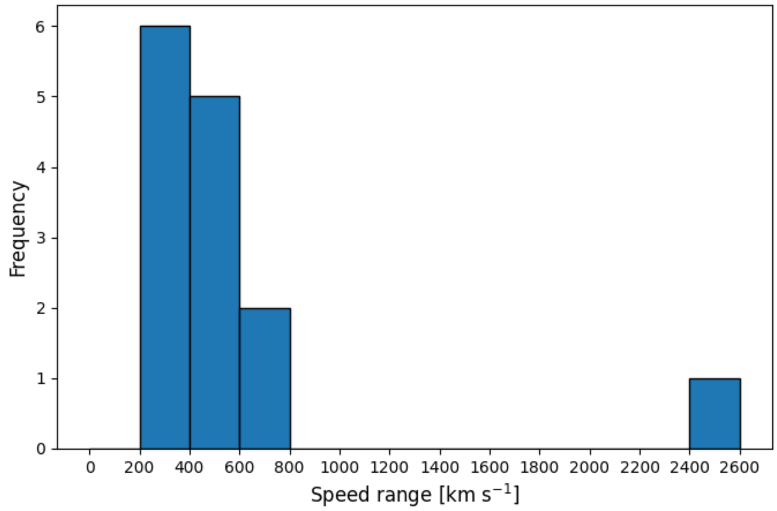

Figure 1. *The 2D "projected" in the plane of the sky velocity distribution of the CMEs included in this study.*

The 3D velocities were calculated upon measuring the CMEs using the images from 2 spacecraft simultaneously. Depending on the visibility of each event in the field of view of the spacecraft, we created combinations of instruments which allowed for the most precise measurements for the longest possible period. For 2/14 events the data from STEREO Behind was absent, and for 2/14 there were gaps in data from LASCO C2 and C3 instruments. The number of CMEs measured with different combination of instruments is listed in Table 1.

Table 1. *Number of the cases in which we chose to use each combination of instruments to measure the 3D velocity of a CME.*

Combination of instruments	No. of events
STEREO A + STEREO B	6
STEREO A + LASCO C2	1
STEREO A + LASCO C3	2
STEREO B + LASCO C2	2
STEREO B + LASCO C3	3

The "true" velocities obtained from different combinations of instruments are shown in Figure 2. At first glance, the distribution resembles that of the 2D velocities measured by the SOHO coronagraph observations. A slight shift towards higher velocities is noticeable, with no event with a velocity <200 km s^{-1}, and the largest number (6/14) of the CMEs having velocities in the range 400-600 km s^{-1}. The fastest ejection of matter is at a velocity of 2600-2800 km s^{-1} (instead of 2400-2600 km s^{-1} for the 2D velocities).

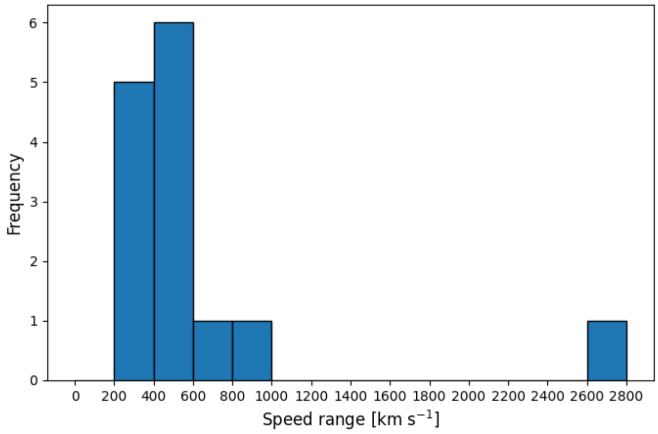

Figure 2. *Distribution of the "true" velocities of the explored sample of CMEs.*

To compare the results, we created a V_{2D} vs. V_{3D} scatter plot (Figure 3), showing a small deviation from y=x line. This indicates a near-linear relationship where the velocities tend to increase together, but not perfectly proportionally. In fact, the trend of the "true" velocities show that they tend to increase more sharply and show larger deviation as 2D speed increase. Events with lower speeds also show smaller deviations.

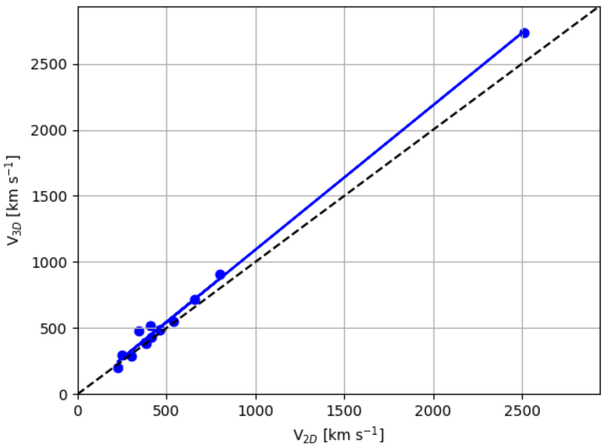

Figure 3. *Comparison between the plane-of-the-sky and "true" velocities of CMEs.*

Estimating Pearson correlation coefficient ($r = 1.0$) we found an extremely strong linear correlation between plane-of-sky (2D) and "true" (3D) CME speeds with 99.5% of the variance in the 3D speeds explained by the 2D measurements (coefficient of determination $r^2 = 0.995$). This indicates that 2D catalog values provide a really good first-order approximation of CME kinematics, but we should note that the low number of events studied probably also plays a significant role in this result. However, correlation does not imply identity: systematic differences remain between 2D and 3D values, reflecting projection effects. Therefore, while catalog speeds are a good proxy for relative variations in CME kinematics, absolute velocity estimates require 3D reconstruction.

To explore in depth, the differences between the speed of the CME (V_{3D}) and its projection (V_{2D}), we calculated the deviation for each measurement:

$$Deviation\ [\%] = \frac{V_{2D} - V_{3D}}{V_{3D}} \times 100. \quad (1)$$

The created histogram represents the percent of deviation of CMEs’ 3D velocity from the linear one (Figure 4).

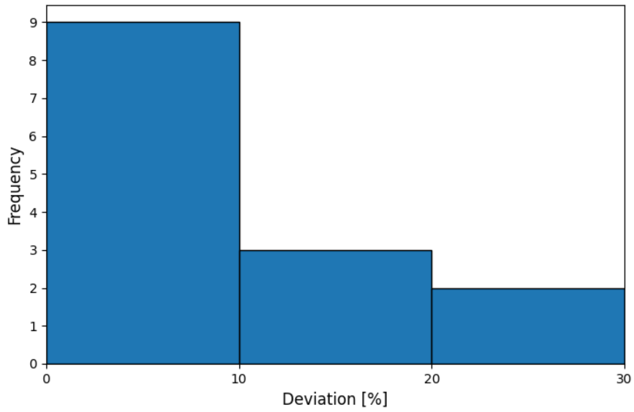

Figure 4. *Distribution of the deviation of the 3D velocities.*

The deviation for 9/14 events (64%) is under 10%, which is another example that the 2D velocities of CMEs are a good representation of the real ones. The two events that show a deviation higher than 20% are the ones from 2012 February 03 and 2013 November 01.

A comparison of CME speeds between events associated with active regions (AR-related) and those originating outside active regions (Non-AR-related) reveals some differences in their distributions. The box plot visualization (Figure 6) indicates that AR-related events exhibit a broader range, including one extreme high-speed outlier (the event from 2012 January 27), which raises their mean speed (803.3 km s^{-1}). In contrast, Non-AR-related CMEs form a more compact distribution, with a lower mean (405.8 km s^{-1}) that is close to their median (490 km s^{-1}). Despite the large difference in mean values, the medians are nearly identical (479 km s^{-1} vs. 490 km s^{-1}), suggesting that typical CME speeds are comparable across the two groups, while AR tend to occasionally produce exceptionally fast CMEs due to the strength and complexity of their magnetic fields.

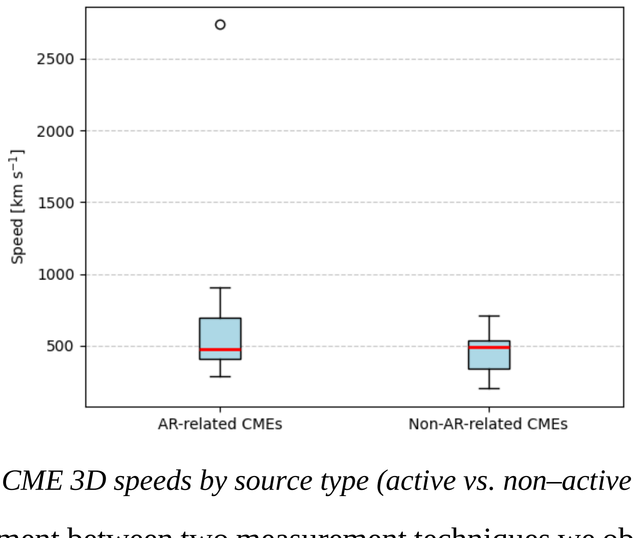

Figure 5. *Boxplot of CME 3D speeds by source type (active vs. non–active regions).*

To assess the agreement between two measurement techniques we obtained a Bland-Altman analysis of the two sets of data – 2D and 3D velocities of the CMEs in our sample (Figure 6). It shows that the catalog (2D) and reconstructed (3D) CME speeds are generally consistent, with most differences lying within ±200 km s^{-1}. The scatter is moderate, with some events exhibiting higher 2D than 3D speeds and others showing the opposite, but all within these bounds. The mean bias is -52.7 km s^{-1}, indicating that 2D speeds are on average ~53 km s^{-1}

lower than their 3D counterparts. Given that the absolute velocities range from several hundred to a few thousand km s^{-1}, this bias is relatively small, corresponding to only a few percent of the typical CME speed.

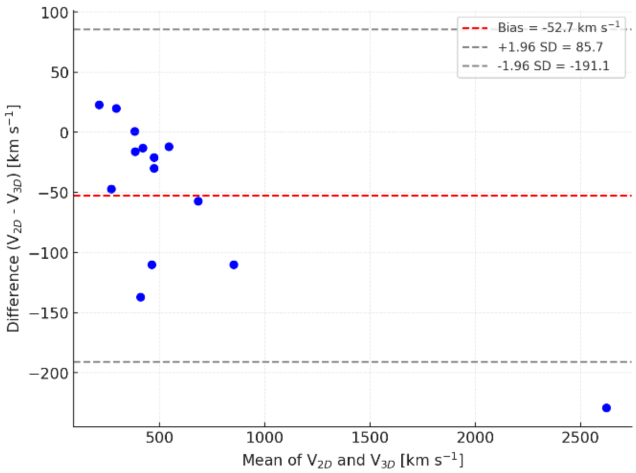

Figure 6. *Bland–Altman plot comparing CME speeds from SOHO/LASCO catalog (2D) and StereoCAT reconstructions (3D). The dashed lines indicate the mean bias (red) and the 95% limits of agreement (grey).*

4. Conclusions

In this work we compared CME plane-of-sky (2D) velocities from the SOHO/LASCO catalog with stereoscopically reconstructed (3D) velocities obtained using the StereoCAT tool for 14 events during Solar Cycle 24. Our results demonstrate that catalog speeds are strongly correlated with the reconstructed ones, indicating that 2D measurements provide a reliable first-order approximation of CME kinematics. Nonetheless, systematic differences persist due to projection effects, with a mean bias of –52.7 km s^{-1} (2D underestimation by only a few percent).

The comparison between AR-related and non-AR-related CMEs shows that while median velocities are similar, AR-associated eruptions occasionally produce extreme high-speed events, thereby elevating their mean values. This highlights the importance of active-region magnetic complexity in driving the fastest CMEs, even though typical velocities across different origins remain comparable.

Despite its usefulness, StereoCAT analysis is subject to limitations, including human selection of tie-points, varying spacecraft viewing geometries, and incomplete data coverage for some events. These factors, together with the relatively small sample size, must be considered when interpreting the results. In order to confirm or disapprove these results, in future we plan a far broader study including events for at least one solar cycle and/or estimating the efficiency of other modeling techniques for reconstruction of CMEs (such as graduated cylindrical shell).

Acknowledgment

This work is supported by the National Science Fund of Bulgaria with contracts No. KP-06-M78/1. We used data from SOHO/LASCO CME Catalog that is generated and maintained at the CDAW Data Center by NASA and The Catholic University of America in cooperation with the Naval Research Laboratory. SOHO is a project of international cooperation between ESA and NASA.

References

Chen, P.F. (2011). Coronal mass ejections: Models and their observational basis, *Living Reviews in Solar Physics*, Vol. 8, 1, DOI: 10.12942/lrsp-2011-1.

Domingo, V., Fleck, B., Poland, A.I. (1995). The SOHO mission: An overview, *Solar Physics*, Vol. 162, pp. 1–37, DOI: 10.1007/BF00733425.

Gopalswamy, N. (2016). History and development of coronal mass ejections as a key player in solar–terrestrial relationship, *Geoscience Letters*, Vol. 3, Art. 8, DOI: 10.1186/s40562-016-0039-2.

Gosling, J.T., Hildner, E., MacQueen, R.M., Munro, R.H., Poland, A.I., Ross, C.L. (1976). The speeds of coronal mass ejection events, *Solar Physics*, Vol. 48, pp. 389–397, DOI: 10.1007/BF00152004.

Howard, R.A., Moses, J.D., Vourlidas, A., et al. (2008). Sun–Earth Connection Coronal and Heliospheric Investigation (SECCHI), *Space Science Reviews*, Vol. 136, pp. 67–115, DOI: 10.1007/s11214-008-9341-4.

Kontogiannis, I. (2023). The characteristics of flare- and CME-productive solar active regions, *Advances in Space Research*, Vol. 71, pp. 2017–2037, DOI: 10.1016/j.asr.2022.10.008.

Low, B.C., Zhang, M. (2002). The hydromagnetic origin of the two dynamical types of solar coronal mass ejections, *Astrophysical Journal*, Vol. 564, L53, DOI: 10.1086/338798.

Mierla, M., Inhester, B., Antunes, A., et al. (2010). On the 3-D reconstruction of coronal mass ejections using coronagraph data, *Annales Geophysicae*, Vol. 28, pp. 203–215, DOI: 10.5194/angeo-28-203-2010.

Sheeley, N.R., Walters, J.H., Wang, Y.-M., Howard, R.A. (1999). Continuous tracking of coronal outflows: Two kinds of coronal mass ejections, *Journal of Geophysical Research: Space Physics*, Vol. 104, 24739, DOI: 10.1029/1999JA900308.

Subramanian, P., Dere, K.P. (2001). Source regions of coronal mass ejections, *Astrophysical Journal*, Vol. 561, No. 1, pp. 372–395, DOI: 10.1086/323213.

Tsvetkov, Ts., Miteva, R., Temmer, M., Petrov, N. (2019). STEREOCat speed de-projection of SEP-related CMEs, *Proceedings of the Eleventh Workshop "Solar Influences on the Magnetosphere, Ionosphere and Atmosphere"*, pp. 207–210, DOI: 10.31401/WS.2019.proc.

Wagner, W.J. (1984). Coronal mass ejections, *Annual Review of Astronomy and Astrophysics*, Vol. 22, No. 1, pp. 267–289, DOI: 10.1146/annurev.aa.22.090184.001411.

Wang, Y., Zhang, J. (2008). A statistical study of solar active regions that produce extremely fast coronal mass ejections, *Astrophysical Journal*, Vol. 680, No. 2, pp. 1516–1522, DOI: 10.1086/587619.

Weber, M.A., Schunker, H., Jouve, L., Işık, E. (2023). Understanding active region origins and emergence on the Sun and other cool stars, *Space Science Reviews*, Vol. 219, No. 8, Art. 63, DOI: 10.1007/s11214-023-01006-5.

Yashiro, S., Gopalswamy, N., Michalek, G., St. Cyr, O.C., Plunkett, S.P., Rich, N.B., Howard, R.A. (2004). A catalog of white light coronal mass ejections observed by the SOHO spacecraft, *Journal of Geophysical Research: Space Physics*, Vol. 109, A07105, DOI: 10.1029/2003JA010282.

Yurchyshyn, V., Yashiro, S., Abramenko, V., Wang, H., Gopalswamy, N. (2005). Statistical distributions of speeds of coronal mass ejections, *Astrophysical Journal*, Vol. 619, 599, DOI: 10.1086/426129.

Appendix

Detailed information about the explored CMEs and the results of the obtained 3D reconstruction is given below in Table 2.

Table 2. *Data for the main parameters of explored events (as given in SOHO LASCO CME Catalog), possible associated phenomena, interval and combination of POVs of instruments used for 3D reconstruction as well as the results and analysis of the obtained reconstruction.*

CME parameters				Sources		Measurements		3D Reconstruction				Analysis
Date	Onset	Angular width	Linear speed	AR	SF	Instru-ments	Interval	Half-width	Speed	Long.	Lat.	Deviation
YYYY-MM-DD	[UT]	[⁰]	[km/s]					[⁰]	[km/s]	[⁰]	[⁰]	[%]
2010-12-06	17:24	82	538			A+C3	19:24-00:24	36	550	-57	-34	-2.2
2011-12-15	4:12	96	304	11374		A+C2	05:30-08:36	25	284	43	-25	7.0
2012-01-27	18:27	360	2508	11402, 11401, 11405	X1.7(17:37) C5.5(06:24) C1.7(01:11)	A+B	18:40-19:39	76	2737	77	28	-8.4
2012-02-03	7:24	177	408			B+C3	09:06-12:09	26	518	-178	-32	-21.2
2012-02-04	18:12	122	656			A+B	19:52-21:54	24	713	-122	-33	-8.0
2012-11-10	14:12	191	460			A+B	16:24-21:39	34	490	131	-34	-6.1
2013-12-04	5:12	60	377	11907, 11906, 11913	C4.7(04:38)	B+C3	06:54-09:39	20	393	75	16	-4.1
2014-02-02	17:24	143	463	11965, 11966		B+C3	19:54-23:26	24	484	117	-43	-4.3
2013-11-01	15:48	184	342	11886		B+C2	16:09-18:39	27	479	146	21	-28.6
2013-11-02	8:24	177	798	11886		A+B	08:54-11:24	46	908	124	43	-12.1
2013-11-03	8:24	98	224			A+B	09:39-19:54	35	201	40	-70	11.4
2013-12-11	7:36	79	383			A+C3	09:18-15:09	33	382	2	-60	0.3
2013-12-27	2:48	77	247			A+B	06:24-14:24	27	294	-29	-62	-16.0
2013-12-29	5:48	215	415	11938, 11937		B+C2	07:24-09:36	39	428	-38	-29	-3.0